Electrospun PLA/PBS/MWCNT nanocomposite fibers for high-performance air filtration: A sustainable approach

Manisara Phiriyawirut*, Prin Wangtanapat, Apiwit Chanthanchumpunon and Ratchanon Phanchaweng

Department of Tool and Materials Engineering, Faculty of Engineering, King Mongkut's University of Technology Thonburi, Bangkok 10140, THAILAND

*Corresponding author: manisara.pee@kmutt.ac.th

ABSTRACT

For the development of high-performance air filtration materials, electrospun polylactic acid (PLA)/polybutylene succinate (PBS) blend fibers, reinforced with multi-walled carbon nanotubes (MWCNTs), were fabricated and subjected to comprehensive characterization. A PLA/PBS blend, at a 95/5 wt% ratio, was prepared through the dissolution of the constituent polymers in a dichloromethane/dimethylformamide mixture, using a 3:1 v/v ratio at a 17 wt% concentration. MWCNTs were introduced into the polymer solution, with dispersion facilitated by a Triton X-100 surfactant and ultrasonication, at concentrations ranging from 0 to 4 wt%. Electrospinning was performed under optimized conditions, specifically an applied voltage of 16 kV and a tip-to-collector distance of 18 cm. Upon the incorporation of MWCNTs, minor alterations to fiber morphology were observed, including a slight increase in fiber diameter and an enhancement in the uniformity of surface pore distribution. Thermal properties were analyzed, revealing a trend of decreasing glass transition temperature, melting temperature, and thermal stability as the MWCNT content increased. Mechanical properties were evaluated, with improvements in tensile strength and Young's modulus documented with increasing MWCNT content. Filtration efficiency was assessed, and significant enhancements were achieved, with performance comparable to N95 masks (98-99%) recorded. Notably, a reduction in pressure drop across the filters was observed with increasing MWCNT content, indicating improved breathability. The potential of these biodegradable and environmentally sustainable nanocomposite fibers as an alternative to conventional filtration materials, addressing the growing concerns surrounding air pollution, is demonstrated by these results. This study highlights the feasibility of employing biopolymers and carbon nanomaterials for a more sustainable approach to air filtration, offering a viable solution for developing advanced, eco-friendly filtration technologies.

Keywords: Electrospinning, Polylactic acid, Polybutylene succinate, Multi-wall carbon nanotube, Filtration

INTRODUCTION

Human health is increasingly jeopardized by air pollution, with fine particulate matter (PM2.5) being a primary concern. Respiratory diseases, cardiovascular issues, and even cancer have been linked to PM2.5 exposure [1]. The urgent need for effective air filtration technologies, as emphasized by the World Health Organization (WHO), is crucial for mitigating these health risks [2]. Conventional filtration materials, such as surgical masks and N95 respirators, offer some protection. However, their reliance on non-biodegradable materials and potential limitations in filtration efficiency, breathability, and long-term sustainability have been noted [3].

As a versatile technique, electrospinning has emerged for the fabrication of nanofibrous membranes across diverse applications, including filtration [4-6]. The high surface area-to-volume ratio and interconnected porous structure inherent in electrospun nanofibers have been observed to be advantageous for capturing fine particulate matter [7]. Numerous studies have explored the capabilities of electrospun nanofibers for air filtration [8]. For example, nanofibers made from polymethyl methacrylate (PMMA) and ethylene vinyl alcohol (EVOH) were fabricated for biofiltration applications, demonstrating excellent filtration efficiency and low pressure drop [9]. Furthermore, polylactic acid (PLA) nanofibers were investigated for air filtration, with their biodegradable nature highlighted as a potential replacement for traditional materials [10].

Biodegradable polymers, notably PLA and polybutylene succinate (PBS), have been considered as promising materials for developing environmentally friendly filtration membranes [11-12]. While PLA offers biodegradability and filtration efficiency, its brittleness and relatively large pore sizes have been acknowledged [13]. Blending PLA with PBS has been shown to mitigate these limitations by improving

mechanical properties and processability. The effects of varying PLA/PBS blend compositions on electrospun fiber properties were studied, revealing a decrease in fiber diameter and an increase in crystallinity upon PBS addition [14]. Additionally, the miscibility of PLA/PBS blends was investigated, with phase separation behavior found to be influenced by blend composition and processing conditions [15]. The compatibility between PLA and PBS, and their ability to form miscible blends, has been well-established [16].

The incorporation of nanomaterials into electrospun polymer matrices has been observed to enhance membrane properties [17-19]. Carbon nanotubes (CNTs), particularly multi-walled carbon nanotubes (MWCNTs), have attracted attention due to their unique properties. MWCNTs are known for their exceptional mechanical properties, electrical conductivity, and high aspect ratio, which have been shown to improve filtration efficiency and mechanical strength in composite membranes. Furthermore, the dispersion of MWCNTs within the polymer solution during electrospinning can be improved by the incorporation of MWCNTs, leading to more uniform fibers [20-21]. The influence of MWCNTs on electrospun polyurethane (PU) fiber properties was investigated, showing that MWCNTs affected PU crystallinity and improved nanofiber properties [22]. Gas barrier properties of electrospun PLA/PBS blend fibers were also investigated, with MWCNTs improving barrier properties, especially for smaller gas molecules [23].

The improvement of mechanical properties and filtration performance of electrospun nanofibers by MWCNTs has been extensively studied [24-26]. However, MWCNT dispersion within the polymer matrix remains challenging due to strong van der Waals interaction. To address this, surfactants have been employed. The effectiveness of nonionic surfactants in MWCNT dispersion in epoxy composites was demonstrated, with Triton X-100 showing significant effectiveness [27]. Similarly, the use of Triton X-100 was reported to significantly improve CNT dispersion in polyvinyl pyrrolidone (PVA) solutions [28].

Significant research has been conducted on the biocompatibility of CNT-polymer composites for various biomedical applications, such as tissue engineering scaffolds and drug delivery systems [29]. These studies often demonstrate that when CNTs are well-dispersed and embedded within a biocompatible matrix, they can exhibit acceptable biocompatibility profiles with minimal cytotoxic effects.

This research investigates the fabrication and characterization of electrospun PLA/PBS nanocomposite fibers reinforced with multi-walled carbon nanotubes (MWCNTs) for high-performance air filtration applications. To facilitate MWCNT dispersion, Triton X-100 is employed. The influence of MWCNT content on fiber morphology, thermal characteristics, mechanical behavior, and filtration performance is systematically evaluated. The development of biodegradable air filtration materials exhibiting high performance is anticipated to contribute to sustainable solutions for air pollution mitigation.

MATERIALS AND METHODS

Materials

For the preparation of nanocomposite fibers, the following materials were utilized: Polylactic acid (PLA), specifically the 042D grade, was obtained from NatureWorks LLC. Polybutylene succinate (PBS), identified as BioPBS FZ91PM grade, was provided by PTT MCC BIOCHEM CO., LTD. Multi-walled carbon nanotubes (MWCNTs) were sourced from Nano Generation Co., Ltd. To facilitate MWCNT dispersion, the surfactant Triton X-100 (Polyoxyethylene octyl phenyl ether) was acquired from Alfa Aesar. Dimethylformamide (DMF) and dichloromethane (DCM) solvents were procured from RCI Labscan Limited.

Polymer solution preparation

A solvent mixture, consisting of dichloromethane (DCM) and dimethylformamide (DMF) in a 3:1 volumetric ratio, was prepared. Polylactic acid (PLA) and polybutylene succinate (PBS) were individually dissolved in this mixed solvent at a concentration of 17 wt%. PLA was dissolved at 100°C, while PBS was dissolved at 150°C. Both solutions were subjected to continuous stirring for 24 hours to ensure complete dissolution. Subsequently, the PLA and PBS solutions were combined at a weight ratio of 95:5 and stirred for an additional 24 hours at 100°C. To enhance MWCNT dispersion, Triton X-100 surfactant was added to the PLA/PBS solution at a 1 wt% concentration and stirred for 20 minutes at 100°C. Varying concentrations of MWCNTs (0, 1, 2, 3, and 4 wt%) were then incorporated into the solution and stirred for 24 hours at 100°C. To achieve a homogeneous dispersion of MWCNTs, the resultant solutions were subjected to high-intensity ultrasonication at frequency of 50-60 Hz for 5 minutes.

Electrospinning process

Electrospinning was employed to fabricate the nanofibers. The prepared polymer solutions containing varying concentrations of MWCNTs (0, 1, 2, 3, and 4 wt%) were loaded into a syringe pump and fed through a stainless-steel needle. A high voltage of 16 kV was applied between the needle tip and a grounded collector, which was placed 18 cm away. The electrospinning process was conducted at room temperature.

Characterization

Viscosity and electrical conductivity: The viscosity of the polymer solutions was determined using a Brookfield DV-III ULTRA rotational viscometer, while the electrical conductivity of the solutions

was measured using a Hach HQD HQ40d conductivity meter. Both measurements were conducted at room temperature.

Morphology: The surface morphology of the electrospun fibers was examined using a JEOL JSM-6610 LV scanning electron microscope (SEM). Prior to imaging, samples were sputter-coated with a thin layer of gold to enhance electrical conductivity. Fiber diameter and pore size were subsequently determined from the SEM micrographs using ImageJ software.

Crystal structure: The crystalline structure of the electrospun fibers was analyzed by X-ray diffraction (XRD) using a Bruker axx D8 DISCOVER diffractometer. XRD patterns were obtained within a 2θ range of 5° to 55° to identify crystalline phases present in the samples.

Thermal properties: Thermal properties of the electrospun fibers were evaluated using differential scanning calorimetry (DSC, NETZSCH DSC 204 F1 Phoenix) and thermogravimetric analysis (TGA, NETZSCH TG 209 F3 Tarsus). DSC measurements, conducted under a nitrogen atmosphere at a heating and cooling rate of 10°C/min within a temperature range of -60 to 230°C with a nitrogen flow rate of 50 mL/min, determined the glass transition temperature (Tg), melting temperature (Tm), and degree of crystallinity. Thermal stability was assessed using TGA, performed under a nitrogen atmosphere at a heating rate of 10 °C/min from 25 to 600°C with a nitrogen flow rate of 20 mL/min.

Mechanical properties: Tensile strength of the electrospun fibers was measured according to ASTM D882-02 using a TA.XT plus C universal testing machine.

Filtration Performance Testing: The filtration efficiency of the electrospun PLA and PLA/PBS/MWCNT composite fibers was determined using a TSI DustTrak 8533 aerosol monitor. Di-ethyl-hexyl-sebacate (DEHS) particles, with a size range of 0.2 to 0.3 micrometers, were generated using an ATM226 aerosol generator. Circular filter samples, 6 cm in diameter and 0.15 ± 0.5 mm in thickness, were placed in a custom-built test rig. The airflow rate through the filter was maintained at 4 liters per minute. The filtration efficiency (η) was calculated based on the upstream and downstream particle concentrations measured by the DustTrak monitor and was determined using equation 1. Here, C_{left} represents the concentration of particles upstream of the filter and C_{right} represents the concentration downstream. The pressure drop across the filter (ΔP) was determined by measuring the change in water level in a manometer connected to the filter holder (ΔH) using equation 2. The filtration efficiency and pressure drop of the electrospun fibers were then compared to those of commercial N95 and surgical masks.

$$\eta = \frac{C_{left} - C_{right}}{C_{left}} \times 100\% \qquad (1)$$

$$\Delta P = \frac{101,325 \text{ Pa} \times \Delta H}{10 \text{ mH}_2\text{O}} \qquad (2)$$

RESULTS AND DISCUSSION

Viscosity of Polymer Solutions

Solution viscosity, a critical parameter influencing electrospinning behavior, was measured at room temperature using a rotational viscometer. The viscosity of the 17 wt% PLA solution was determined to be 36.48 ± 0.2 cP, as presented in Table 1. A slight reduction in viscosity, to 33.8 ± 0.1 cP, was observed upon the incorporation of PBS into the PLA solution. This minor decrease is attributed to the enhanced compatibility between the PLA and PBS polymers. It is suggested that the introduction of PBS may have led to a slight disruption in the PLA chain entanglements, thereby lowering the overall resistance to flow. This observation is consistent with previous studies that have documented the improved miscibility of PLA and PBS blends, leading to a more homogeneous solution.

Table 1 Viscosity and electrical conductivity of pure PLA. Pure PBS, PLA/PBS and PLA/PBS/MWCNT solutions.

Sample	Viscosity (cP)	Electrical Conductivity (μS/cm)
PLA	36.5 ± 0.2	1.96 ± 0.01
PBS	N/A	1.55 ± 0.01
PLA/PBS	33.8 ± 0.1	2.59 ± 0.01
PLA/PBS/MWCNT-1	35.3 ± 0.0	97.5 ± 0.01
PLA/PBS/MWCNT-2	38.7 ± 0.2	231 ± 0.01
PLA/PBS/MWCNT-3	44.6 ± 0.2	332 ± 0.01
PLA/PBS/MWCNT-4	51.6 ± 0.2	382 ± 0.01

A noticeable increase in solution viscosity was recorded upon the incorporation of multi-walled carbon nanotubes (MWCNTs). Specifically, the viscosity of the PLA/PBS/MWCNT solutions was found to range from 35.2 ± 0.1 cP to 51.58 ± 0.2 cP, with the variation directly corresponding to the MWCNT content. This increase in viscosity is attributed to the development of a three-dimensional network within the solution. This network formation is believed to be facilitated by the high aspect ratio and substantial surface area characteristics of MWCNTs. The increased interactions between the MWCNTs, PLA, and PBS molecules, including van der Waals forces and π-π interactions, are thought to contribute to viscosity enhancement. These results are consistent with findings reported in previous investigations [23], where it was demonstrated that the introduction of MWCNTs into polymer solutions led to an increase in viscosity, presumably due to the creation of a more entangled polymer network. It is

suggested that the increased viscosity directly impacts the electrospinning process, possibly leading to changes in fiber morphology and uniformity.

Electrical conductivity of polymer solutions

Electrical conductivity measurements were performed on the prepared polymer solutions at room temperature, with the exception of the PBS solution, for which measurements were taken at 50°C to prevent solidification. The conductivity values obtained for PLA, PBS, PLA/PBS, and PLA/PBS/MWCNT solutions are presented in Table 1.

A conductivity of 1.96 ± 0.01 μS/cm was measured for the PLA solution, while the PBS solution exhibited a slightly lower conductivity of 1.55 ± 0.01 μS/cm. An increase in conductivity to 2.59 ± 0.01 μS/cm was observed upon blending PLA with PBS. The increase in conductivity observed upon blending PLA with PBS can be attributed to several factors related to the miscibility and interaction between the two polymers, as well as the potential presence of ionic impurities within each polymer that become more mobile or concentrated at the interface upon blending. However, the most significant enhancement in electrical conductivity was achieved with the incorporation of MWCNTs. The conductivity of the PLA/PBS/MWCNT solutions ranged from 97.5 ± 0.01 to 382 ± 0.01 μS/cm, dependent upon the MWCNT content.

This substantial increase in conductivity is believed to be the result of a conductive network formed within the polymer matrix. The MWCNTs, acting as conductive fillers, facilitate electron transport, thereby enhancing the overall conductivity of the composite. It is suggested that this finding aligns with previous research [30], where a similar increase in electrical conductivity was reported upon the addition of MWCNTs to polymer matrices. The formation of a conductive network was likely aided by the high aspect ratio of the MWCNTs and their ability to create interconnected structures within the polymer blend.

Morphology of electrospun fibers

The visual appearance of the electrospun fibers is presented in Figure 1. A white, opaque appearance was observed for the electrospun PLA fibers, suggesting a structure that appeared dense and possibly non-porous to the naked eye. The PLA/PBS blend fibers displayed a similar visual morphology to the pure PLA fibers. However, with the introduction of MWCNTs, a noticeable color change was observed. The fiber mats transitioned from a white hue to a dark gray, with the intensity of the gray coloration becoming progressively more pronounced as MWCNT content was increased. This gradual darkening was taken as a clear visual indication of the successful incorporation and increasing concentration of MWCNTs within the PLA/PBS polymer matrix.
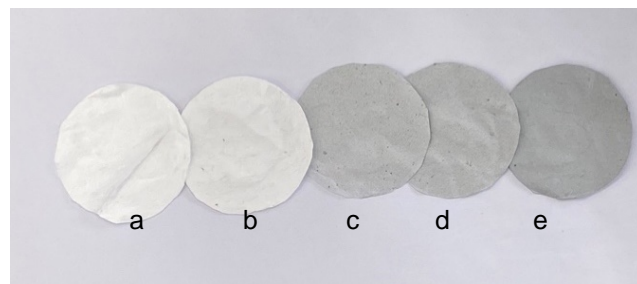

Figure 1 Visual appearance of electrospun fibers: (a) Pure PLA, (b) PLA/PBS, and PLA/PBS/MWCNT composites with varying MWCNT concentrations: (c) 1 wt%, (d) 2 wt% and (e) 3 wt%.
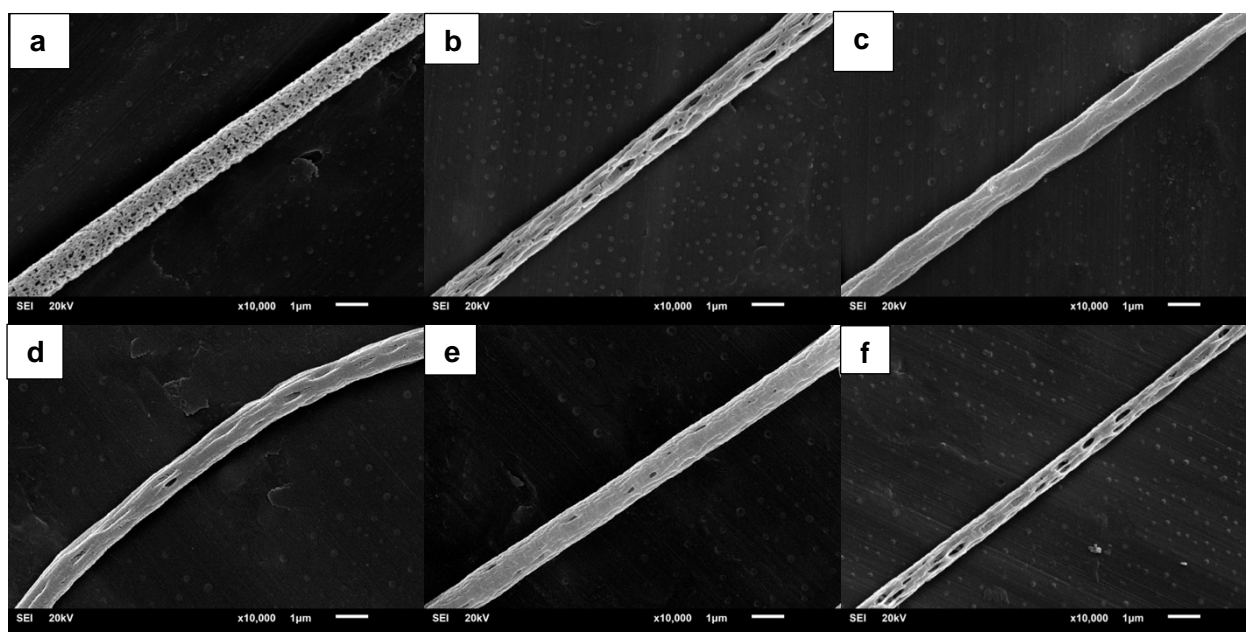

Figure 2 SEM images of electrospun fibers: (a) Pure PLA, (b) PLA/PBS, and PLA/PBS/MWCNT composites with varying MWCNT concentrations: (c) 1 wt%, (d) 2 wt%, (e) 3 wt%, and (f) 4 wt%. Scale bar: 1 μm.

It should be clarified that, owing to challenges encountered in detaching the fiber mat containing 4 wt% MWCNT from the aluminum foil substrate without significant damage, XRD analysis, mechanical property evaluation, and filtration performance testing could not be performed on this specific composition. This strong adhesion may be attributed to an enhanced interaction between the MWCNTs and the substrate, potentially resulting from a combination of significant Van der Waals forces arising from the extensive contact area and mechanical interlocking of the nanofiber network with the aluminum foil's surface. Furthermore, due to the high melting temperature and crystallinity of PBS, the electrospinning of pure PBS fibers proved challenging under the chosen processing conditions. Consequently, the morphology of pure PBS fibers was not investigated in this study.

Distinct morphological features of the electrospun PLA, PLA/PBS, and PLA/PBS/MWCNT fibers were observed through scanning electron microscopy (SEM) and are presented in Figure 2. Pure PLA fibers, as imaged, displayed a characteristic bead-on-string morphology, punctuated by micro-sized pores. The formation of these pores is believed to be a consequence of rapid solvent (DCM/DMF) evaporation during the electrospinning process. Upon blending PLA with PBS, a morphology similar to pure PLA was noted, though pores with slightly elongated shapes were evident. The increased flexibility imparted by PBS to the PLA matrix is thought to have facilitated this elongation.
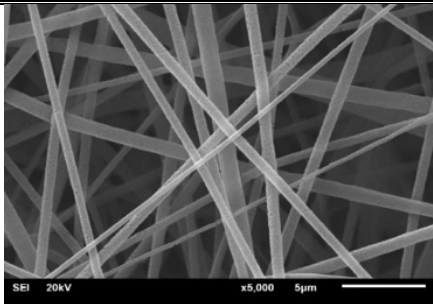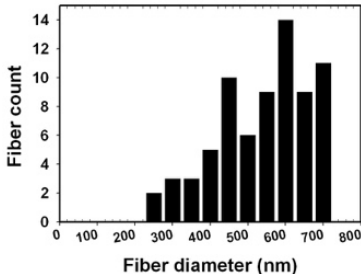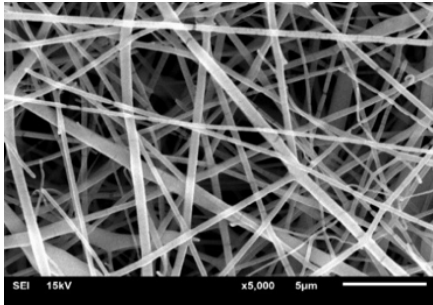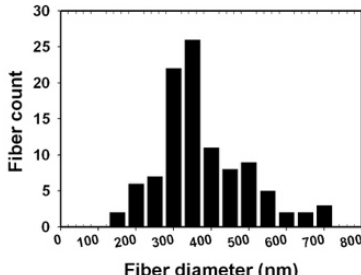
A notable impact on fiber morphology was observed with the incorporation of MWCNTs into the PLA/PBS blend. MWCNTs appeared to function as nucleation sites, promoting the formation of more uniform and well-defined pores. With increasing MWCNT content, the pore distribution along the fiber surface became increasingly uniform, and the pores themselves exhibited greater elongation. This behavior is attributed to the improved mechanical properties of the composite fibers, which are thought to have allowed them to withstand greater stretching forces during electrospinning. Furthermore, the increased viscosity of the polymer solution, a result of MWCNT addition, is believed to have contributed to the formation of finer and more uniform fibers. These morphological changes are consistent with findings reported in previous studies, where the introduction of nanofillers has been shown to significantly influence electrospun fiber morphology [31].

It was found that the MWCNTs are typically embedded and physically entrapped within the polymer matrix (PLA/PBS in this case). This strong physical integration significantly limits the potential for the release of free CNTs during normal use of the filter. The polymer acts as a binder, effectively immobilizing the nanofiller.

The average fiber diameter and diameter distribution for the PLA and PLA/PBS/MWCNT composite fibers, as determined from SEM images, are summarized in Table 2. Pure PLA fibers exhibited an average diameter of 669 nm. The addition of PBS to the PLA matrix resulted in a decrease in the average fiber diameter to approximately 390 nm. This reduction in fiber diameter can be attributed to the improved processability of the PLA/PBS blend, which is likely due to the enhanced compatibility between the two polymers.

Table 2 Fiber morphology and diameter distribution of electrospun pure PLA, PLA/PBS, and PLA/PBS/MWCNT fibers.

Sample	SEM image (500x)	Diameter distribution	Average diameter (nm)
PLA			669±270
PLA/PBS			390±180

Sample	SEM image (500x)	Diameter distribution	Average diameter (nm)
PLA/PBS/MWCNT-1			440±140
PLA/PBS/MWCNT-2			430±240
PLA/PBS/MWCNT-3			420±160
PLA/PBS/MWCNT-4			370±210

* Electrospinning conditions: 16 kV, 18 cm tip-to-collector distance, 90 min spinning time.

The sample designation "PLA/PBS/MWCNT-x" indicates the weight percentage concentration of multi-walled carbon nanotubes (MWCNTs) within the PLA/PBS blend. For instance, the notation "PLA/PBS/MWCNT-1" denotes an MWCNT concentration of 1 wt%.

Upon incorporation of MWCNTs, a slight increase in diameter was detected when compared to the pure PLA/PBS blend, despite an observed increase in solution viscosity. This seemingly contradictory result can be attributed to the interplay between viscosity and electrical conductivity. While an elevated viscosity is generally understood to yield thicker fibers, the enhanced electrical conductivity imparted by MWCNTs has been shown to facilitate the formation of thinner fibers. This is due to an increase in Coulombic repulsion and electrostatic forces within the electrospinning jet. This phenomenon, where competing forces influence fiber diameter, has been documented in prior research [32]. The final fiber diameter, therefore, is determined by the equilibrium established between these opposing forces.

Furthermore, a trend toward a slight decrease in average fiber diameter was noted at higher MWCNT loadings. This reduction can be rationalized by the formation of a more conductive network within the polymer matrix. This network, in turn, facilitates the elongation of the Taylor cone during the electrospinning process, resulting in the production of thinner fibers. This observation aligns with findings reported by Xin and Chen [33], wherein a similar trend was observed

during the electrospinning of polysulfonamide (PSA) solutions containing MWCNTs. The established conductive network allows for the efficient transfer of charge, increasing the stretching force applied to the jet.

Crystal structure analysis

The crystalline structure of the electrospun fibers was examined through X-ray diffraction (XRD) analysis. Illustrated in Figure 3 illustrates the obtained XRD patterns for pure PLA, PBS, and the PLA/PBS/MWCNT composite fibers.

A characteristic peak at 2θ = 16.9° was observed in the XRD pattern of pure PLA, correlating with the crystalline structure of PLA as documented in prior research [34]. Similarly, peaks at 2θ = 19.5 and 22.5° were identified in the XRD pattern of pure PBS, aligning with findings from previous PBS studies [34]. A distinct peak at 2θ = 25.7°, associated with the (002) plane of the graphitic structure, was recorded for the MWCNTs [35].
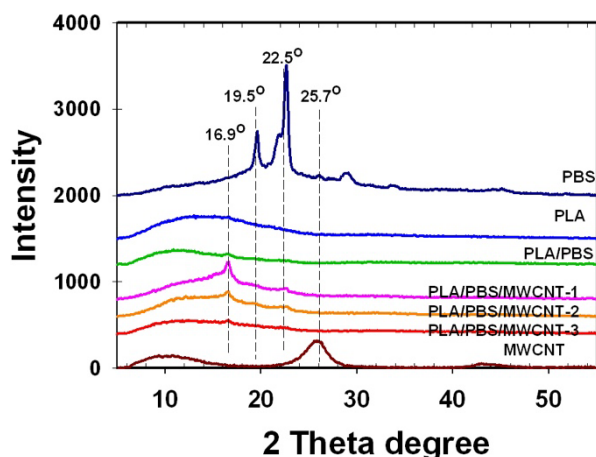

Figure 3 XRD patterns of MWCNT, electrospun pure PLA, pure PBS, PLA/PBS and PLA/PBS/MWCNT fibers.

Within the PLA/PBS/MWCNT composite fibers, the presence of the characteristic PLA peak at 2θ = 16.9° was confirmed. A slight increase in the intensity of this PLA peak was noted with the addition of 1 wt% MWCNTs, suggesting a slight enhancement in PLA crystallinity. However, as MWCNT content was further increased, a reduction in the PLA peak intensity was observed, indicating a decrease in crystallinity. This phenomenon is thought to stem from the nucleation effect of MWCNTs. At lower MWCNT concentrations, the MWCNTs appear to function as nucleation sites, facilitating PLA crystallization. Conversely, at elevated concentrations, the MWCNTs may impede polymer chain mobility, thereby limiting overall crystallinity. This behavior bears resemblance to the results presented by Xin and Chen [33], where a decrease in polysulfonamide fiber crystallinity was reported with increasing MWCNT content.

Thermal properties

The thermal behavior of the electrospun fibers was examined using differential scanning calorimetry (DSC), with key thermal transitions shown in Figure 4 and summarized in Table 3.
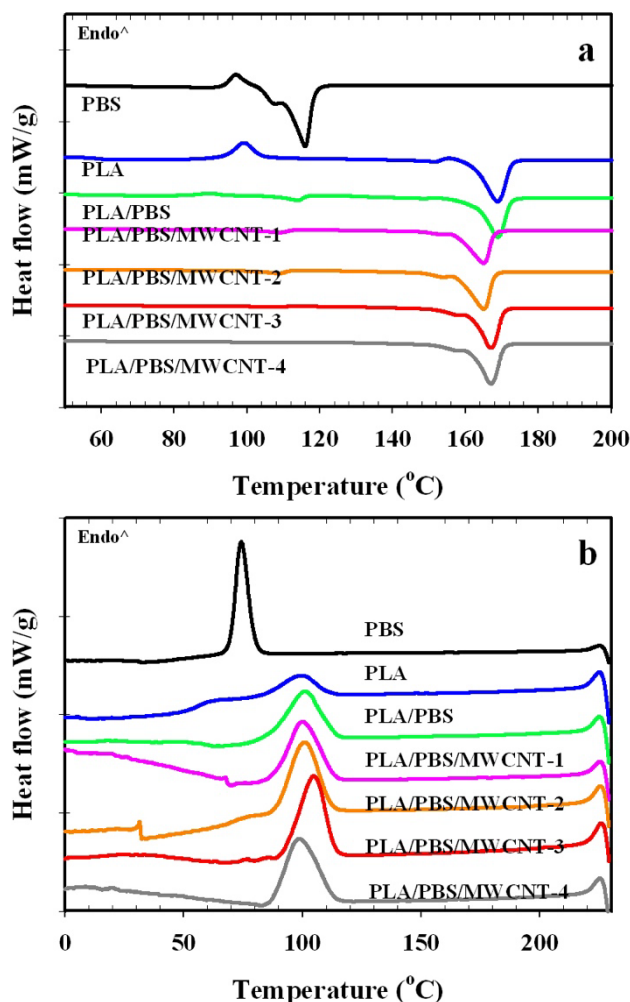

Figure 4 DSC thermogram of electrospun pure PLA, pure PBS, PLA/PBS and PLA/PBS/MWCNT fibers. (a) Heating scan and (b) Cooling scan.

The glass transition temperature (T_g) of PLA was determined to be 62.3°C. Conversely, a distinct T_g for PBS was not discernible within the measured temperature range. This absence is consistent with the reported low T_g of PBS, which is -31.2°C [14]. A single T_g, observed at 62°C, was recorded for the PLA/PBS blend, indicating good miscibility between the two polymers. This single T_g value was found to be in agreement with findings by Phiriyawirut et al. [14], who also reported a single T_g for PLA/PBS blends. It should be noted that while Phiriyawirut et al. observed a decrease in T_g with increasing PBS content, no such decrease was observed in the present study. This discrepancy is likely attributable to the low PBS content (5 wt%) used. However, the addition of MWCNTs to the PLA/PBS blend resulted in a decrease in T_g. This trend aligns with observations made by Yuen [36], who reported a decrease in T_g with

increasing MWCNT content in polyimide composites. Yuen attributed this reduction to the non-polar nature of MWCNTs, which, when incorporated, weakens interactions with the polymer matrix. This weakening is thought to lead to increased free volume and, consequently, enhanced mobility of the polymer chains.

The crystallization temperature (T_c) was measured at 99.6°C for PLA and 74.2°C for PBS. For the PLA/PBS blend, the T_c of PLA was observed at 101.1°C. The incorporation of MWCNTs into the PLA/PBS blend did not appear to significantly alter the T_c of PLA, with values ranging from 98.6 to 104.8°C. The T_c of PBS was not detected in the blends, likely due to its low concentration.

The melting temperature (T_m) of PLA was 159.5°C, and that of PBS was 103.8°C. The PLA/PBS blend showed two T_m values, one at 108.2°C corresponding to PBS and the other at 158.5°C corresponding to PLA. The addition of MWCNTs to the PLA/PBS blend resulted in a decrease in both T_m values, shifting to 102.6°C for PLA and 152°C for PBS. This decrease in T_m is consistent with the findings of Chow et al. [37], who reported a similar decrease in T_m for PLA/PP electrospun fibers with the addition of MWCNTs. They attributed this phenomenon to the high thermal conductivity of MWCNTs, which can act as nucleating agents and facilitate heat distribution within the fibers, leading to a reduction in the melting temperature.

The crystallinity of the electrospun fibers was investigated using DSC. Pure PLA fibers exhibited a crystallinity of 50.70%, while PBS fibers showed a crystallinity of 34.26%. The PLA/PBS blend fibers had a crystallinity of 51.19%, indicating that the addition of PBS did not significantly alter the crystallinity of PLA in the blend. This result differs from the findings reported by Phiriyawirut et al. [14], who observed an increase in PLA crystallinity in PLA/PBS blends due to the nucleating effect of PBS. They also noted a tendency for decreased crystallinity with increasing PBS content. The nucleating effect of PBS on PLA crystallinity, as reported by Phiriyawirut et al. [14], is strongly dependent on the interfacial interactions between the constituent polymers. These interactions can be influenced by the molecular weight of both components. Variations in molecular weight could lead to differences in the degree of mixing, phase morphology, and the nature of the interface, consequently affecting the effectiveness of PBS as a nucleating agent for PLA. Therefore, despite a potentially similar blend ratio, the differing molecular weights of the PLA and PBS components between this study and that of Phiriyawirut et al. [14] likely play a crucial role in the observed discrepancies in PLA crystallinity within the blend. Chain mobility, interfacial interactions, and the effectiveness of PBS as a nucleating agent for PLA are all influenced by molecular weight.

Table 3 Thermal transition temperatures and crystallinity of electrospun pure PLA, pure PBS, PLA/PBS and PLA/PBS/MWCNT fibers.

Sample	T_g (°C)	T_c (°C)	T_m (°C)		ΔH_m (J/g)		X_c (%)	
			PBS	PLA	PBS	PLA	PBS	PLA
PLA	62.3	99.6	-	159.5	-	47.51	-	50.70
PBS	-	74.2	103.8	-	68.52	-	34.26	-
PLA/PBS	62	101.1	108.2	158.5	4.48	50.5	0.11	51.19
PLA/PBS/MWCNT-1	58.2	100.1	102.6	152	2.93	59.2	0.06	59.19
PLA/PBS/MWCNT-2	53.5	100.8	100.6	146	3.17	41.89	0.04	41.57
PLA/PBS/MWCNT-3	53.1	104.6	101.3	148	3.88	49.01	0.03	48.12
PLA/PBS/MWCNT-4	56.4	98.6	96	151	1.21	52.03	0.01	50.53

The addition of MWCNTs at 1 wt% increased the crystallinity of the PLA/PBS blend to 59.19%. This increase in crystallinity with the addition of 1 wt% MWCNTs can be explained by the nucleating effect of MWCNTs. This observation is consistent with the research by Ceregatti [38] on the thermal and electrical properties of PLA/CNT composites, where the percentage of PLA crystallinity increased with increasing MWCNT content. Ceregatti attributed this increase to the higher concentration of nanoparticles providing a greater number of nucleation sites. MWCNTs act as heterogeneous nucleation sites, accelerating the crystallization of PLA.

However, further increasing the MWCNT content from 1 wt% to 4 wt% in the PLA/PBS blend led to a decrease in crystallinity. This decrease at higher MWCNT loadings is likely due to the agglomeration of MWCNTs, which hinders their ability to act as effective nucleating agents. The observed agglomeration at 4 wt% MWCNT suggests that the combination of the Triton X-100 concentration and the ultrasonication conditions employed may not have been sufficient to effectively overcome strong inter-nanotube attractions and maintain a stable, well-dispersed state at this higher loading. Consequently, improved dispersion at higher MWCNT loadings might necessitate a higher surfactant concentration, optimized ultrasonication

parameters (e.g., higher power, longer duration, pulsed sonication), or the incorporation of a different or additional dispersing agent. The observed decrease in crystallinity with increasing MWCNT content in this DSC study is also consistent with the XRD results, where the intensity of the PLA peak at $2\theta = 16.9°$ decreased with increasing MWCNT content. This correlation between DSC and XRD data further supports the conclusion that MWCNT dispersion plays a crucial role in influencing the crystallinity of the PLA/PBS/MWCNT composite fibers. Ghane et al. [39] also found a similar trend in their work on electrospun polyamide-6/MWCNT nanocomposite fibers and films, where the enthalpy of melting (ΔH_m), and thus the degree of crystallinity (X_c) increased with increasing MWCNT content up to a certain point, beyond which further increases in MWCNT led to a decrease in crystallinity. This was attributed to the role of MWCNTs as nucleating agents at lower concentrations, promoting the formation of ordered 3D structures around their axes, while at higher concentrations, agglomeration hinders this effect.
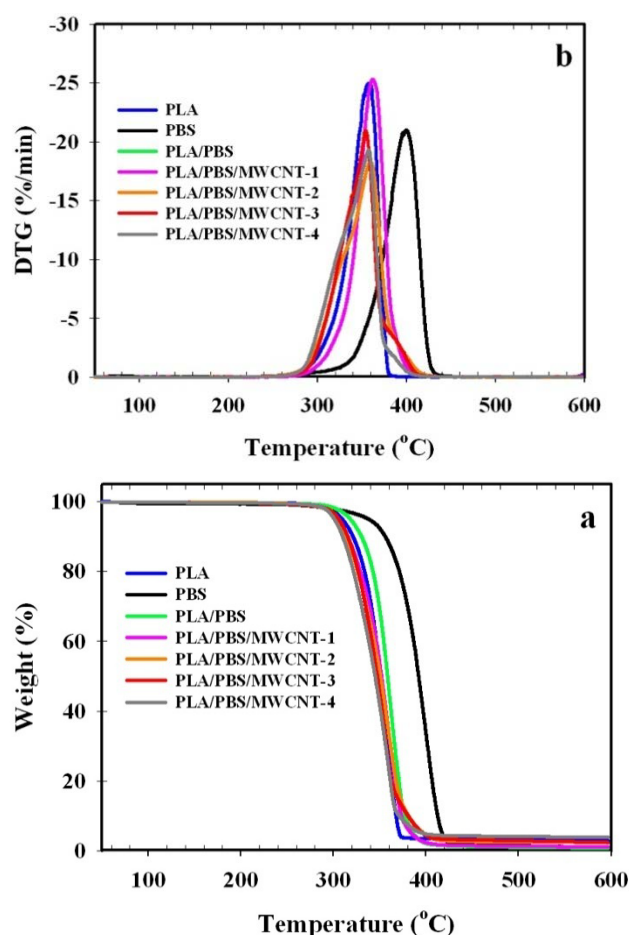

Figure 5 TGA analysis of electrospun pure PLA, pure PBS, PLA/PBS and PLA/PBS/MWCNT fibers. (a) TGA thermogram and (b) DTG thermogram.

The thermal stability of the electrospun fibers was evaluated through thermogravimetric analysis (TGA), as shown in Figure 5. For each sample, the onset

degradation temperature (T_{onset}) and maximum degradation temperature (T_{max}) were determined. These values, along with the percentage weight loss, are presented in Table 4 for electrospun PLA, PBS, and PLA/PBS blends containing varying MWCNT loadings.

Table 4 Thermal degradation behavior of electrospun pure PLA, pure PBS, PLA/PBS and PLA/PBS/MWCNT fibers.

Sample	T_{onset} (ºC)	T_{max} (ºC)	Weight loss (%)
PLA	330.2	357.2	97.15
PBS	371.8	400.0	98.99
PLA/PBS	339.1	361.8	99.30
PLA/PBS/MWCNT-1	331.8	360.1	98.77
PLA/PBS/MWCNT-2	322.5	359.5	97.54
PLA/PBS/MWCNT-3	327.2	353.8	97.52
PLA/PBS/MWCNT-4	321.4	357.4	96.08

It was observed that pure PLA exhibited a T_{onset} of 330.2°C, while PBS displayed a higher T_{onset} of 371.8 °C. The PLA/PBS blend, however, showed a T_{onset} of 339.1°C. This increase in T_{onset} compared to pure PLA indicates that the addition of PBS contributed to an improvement in the thermal stability of PLA. A similar trend was noted for the T_{max} values, where an increase was observed with the addition of PBS to PLA.

These observations are consistent with previous findings. For instance, Vorawongsagul et al. [40] examined the thermal properties of 80/20 PLA/PBS blends. They reported T_{onset} values of 362°C for PLA and 400°C for PBS. Their study revealed a two-stage degradation process in the PLA/PBS blends, with the first stage attributed to the thermal degradation of PLA and the second stage associated with the decomposition of PBS. In the present study, however, a single degradation step was observed for the PLA/PBS blend. This difference may be attributed to the relatively low PBS content (5 wt%) used, which might not have been sufficient to clearly delineate both degradation stages. The lower PBS content likely resulted in an overlapping degradation profile, making the two distinct stages less apparent.

Within the tested temperature range, no significant degradation of the multi-walled carbon nanotubes (MWCNTs) was observed. This observation aligns with the understanding that MWCNT degradation typically occurs around 800°C [37]. Upon the addition of MWCNTs to the polylactic acid (PLA)/polybutylene succinate (PBS) blend, a decrease in the onset degradation temperature (T_{onset}) was noted as MWCNT content increased. This finding is consistent with observations reported by Chow and Lim [37], who investigated PLA/polypropylene (PP)/MWCNT composites. They found a lowered degradation temperature for the PLA phase within the composites

compared to the PLA/PP blend. This reduction might be explained by the high thermal conductivity of MWCNTs, which can enhance heat transfer and accelerate polymer nanocomposite degradation, thereby lowering the activation energy for the process. Furthermore, given PLA's known susceptibility to thermal degradation, the presence of highly conductive MWCNTs may exacerbate this, enhancing heat dissipation.

A tendency for weight loss to decrease with increasing MWCNT loading was observed in the PLA/PBS blends. This trend suggests that higher MWCNT content contributes to an increase in residual char content post-combustion. This result is consistent with work by Eun et al. [41], who studied polyvinylidene fluoride (PVDF) nanofibers with MWCNTs. They reported a decrease in weight loss with increasing MWCNT content (2 to 10 wt%), attributed to the higher thermal stability of MWCNTs compared to PVDF.

The introduction of MWCNTs into the PLA/PBS blend resulted in a decreased T_{onset}, indicating a reduction in composite fiber thermal stability. This could be attributed to a catalytic effect of MWCNTs on polymer matrix thermal degradation. The high thermal conductivity of MWCNTs may facilitate heat transfer within the composite, accelerating degradation. Additionally, defects and impurities within MWCNTs could serve as initiation sites for thermal degradation.

An increase in composite fiber weight loss with increasing MWCNT content was also observed. This is likely due to the higher thermal stability of MWCNTs, which may act as a barrier, hindering the volatilization of polymer degradation products. Similar observations have been documented in the literature [37, 41].

Mechanical properties

The mechanical properties of the electrospun PLA, PLA/PBS, and PLA/PBS/MWCNT composite fibers were assessed through tensile testing, conducted in accordance with ASTM D882-02 standards. The resulting data, including tensile strength, elongation at break, and Young's modulus, are presented in Figure 6.

For the pure PLA fibers, a tensile strength of 0.42 MPa and a Young's modulus of 7.08 MPa were measured. Upon the introduction of PBS into the PLA matrix, a notable increase in both tensile strength and Young's modulus was observed, with values reaching 0.73 MPa and 8.27 MPa, respectively. This improvement can be attributed to the enhanced chain mobility within the polymer matrix, resulting from the plasticizing effect exerted by PBS. Additionally, a significant increase in elongation at break was recorded for the PLA/PBS blend when compared to pure PLA fibers.
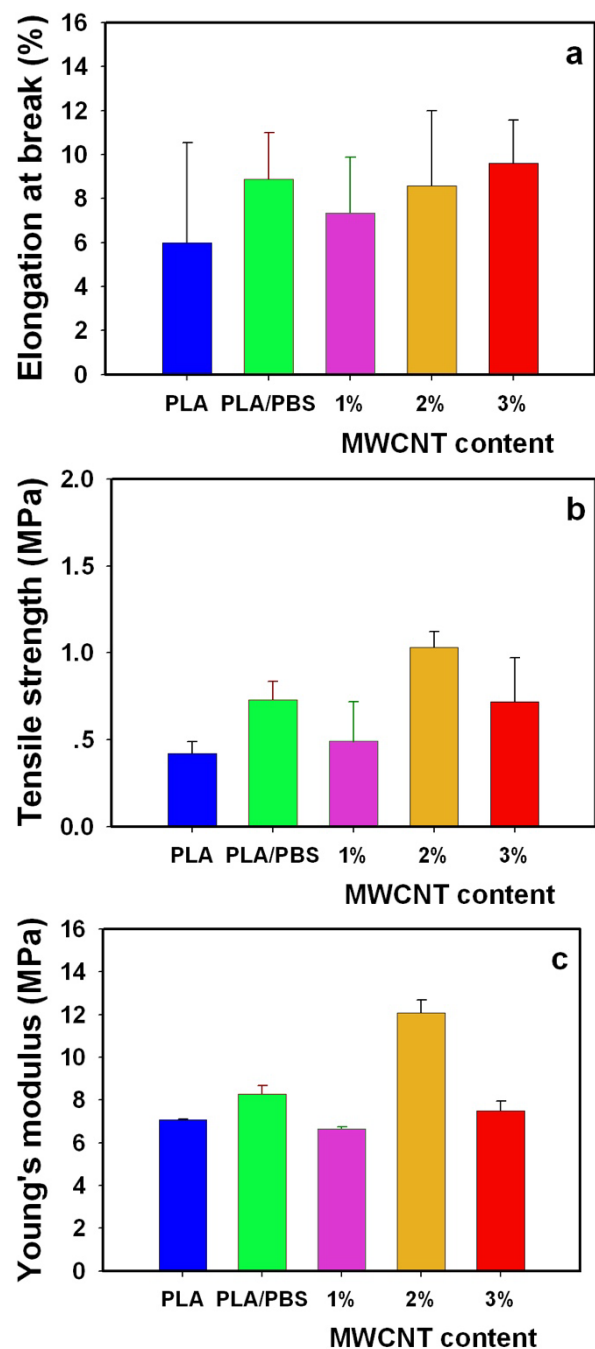

Figure 6 Tensile properties of electrospun pure PLA, PLA/PBS and PLA/PBS/MWCNT fibers (a) Elongation at break, (b) Tensile strength and (c) Young's modulus.

However, the addition of MWCNTs did not yield a statistically significant change in elongation at break. This observation differs from the findings reported by Badar et al. [23]. This discrepancy might be explained by variations in processing conditions, MWCNT loading, or the specific polymer matrix employed in the previous study. Further investigation into these parameters could provide a more comprehensive understanding of the observed differences.

Tensile strength and Young's modulus were evaluated to determine the mechanical performance of the composite fibers. The PLA/PBS blend exhibited

increased tensile strength and Young's modulus compared to pure PLA, consistent with enhanced interfacial adhesion between the PLA and PBS phases, as previously reported [14]. The incorporation of MWCNTs further increased the Young's modulus, indicating enhanced stiffness due to the formation of a more rigid, interconnected MWCNT network that restricts polymer chain deformation.

The influence of MWCNTs on tensile strength was less consistent, displaying variability with MWCNT loading. This behavior is attributed to competing effects of reinforcement and agglomeration. At lower loadings, MWCNTs acted as reinforcing agents, enhancing mechanical properties likely due to effective stress transfer at the MWCNT-polymer interface [23]. However, at higher loadings, MWCNT agglomeration led to stress concentrations and a reduction in tensile strength, a trend also observed by Islam et al. [42].

Filtration efficiency

Filtration efficiency of electrospun PLA, PLA/PBS, and PLA/PBS/MWCNT composite fibers was assessed using a TSI DustTrak 8533 aerosol monitor. Results were then compared with those obtained from commercial surgical masks and N95 respirators. As presented in Table 5, the electrospun fibers demonstrated exceptional filtration performance, reaching levels comparable to N95 masks. Average filtration efficiency for the electrospun fibers was found to range between 98% and 99%, a significant improvement over the 19.5-19.9% efficiency recorded for standard surgical masks.

Table 5 Filtration efficiency and pressure drop of surgical masks, N95 respirators, and electrospun pure PLA, PLA/PBS and PLA/PBS/MWCNT fibers.

Sample	Filtration efficiency (%)	Pressure drop (Pa)
Surgical masks	19.9+2.5	152+11.7
N95 respirators	98.6+0.0	304+58.5
Electrospun fibers		
PLA	99.1+0.2	709+58.5
PLA/PBS	99.2+0.2	1165+50.7
PLA/PBS/MWCNT-1	98.5+1.0	1064+155
PLA/PBS/MWCNT-2	99.1+0.1	963+163
PLA/PBS/MWCNT-3	99.2+0.1	760+183

The high filtration efficiency observed in the electrospun fibers is attributed to several factors. Firstly, a high surface area-to-volume ratio, characteristic of electrospun fibers, provides numerous sites for particle capture. Secondly, the small pore size within the fiber network effectively traps fine particles, including those in the submicron range. Thirdly, an interconnected fibrous network forms a multi-layered filtration barrier, which enhances capture efficiency.

Lastly, the incorporation of MWCNTs provides additional sites for particle capture and improves the mechanical stability of the fibrous mat, further contributing to the enhanced filtration performance.

Breathability, as indicated by pressure drop across the filter materials, was assessed. The pressure drop values obtained for electrospun PLA/PBS/MWCNT composite fibers, alongside commercial surgical masks and N95 respirators, are presented in Table 5. Surgical masks were found to exhibit a pressure drop of 152 Pa, while N95 respirators demonstrated a range from 30 to 304 Pa. In contrast, the electrospun fibers showed pressure drop values ranging from 709 to 1165 Pa. These elevated values suggest that the developed PLA/PBS/MWCNT composite fibers, in their current state, may not be suitable for direct application in personal respiratory masks due to potentially compromised user comfort arising from excessive pressure drop.

The higher pressure drop observed for the electrospun fibers is thought to be a consequence of their denser and more tortuous structure when compared to the nonwoven fabrics utilized in commercial masks. The smaller pore sizes and increased fiber density inherent in electrospun mats are believed to contribute to a greater resistance to airflow, thereby resulting in the elevated pressure drop.

The influence of MWCNT addition on the PLA/PBS blend's pressure drop was shown to be multifaceted. While an increase in fiber diameter and a more elongated pore morphology, associated with increasing MWCNT content, might have been expected to reduce pressure drop, a consistent trend was not observed. This suggests that factors such as fiber orientation and the level of fiber entanglement may have played a significant role in determining the pressure drop.

It has been established in previous studies that fiber morphology, including fiber diameter, pore size distribution, and fiber orientation, can significantly affect the airflow resistance of nonwoven fabrics [43]. Generally, smaller fiber diameters and a narrower pore size distribution are associated with higher pressure drops. However, the complex interactions between these factors, coupled with the unique characteristics of the electrospun fibers, make it challenging to accurately predict the precise relationship between fiber morphology and pressure drop.

CONCLUSIONS

This study successfully fabricated and characterized electrospun PLA/PBS composite fibers reinforced with MWCNTs for high-performance air filtration. The incorporation of MWCNTs enhanced electrical conductivity, mechanical strength, and filtration efficiency. Notably, increased polymer solution viscosity with 1-3 wt% MWCNT led to a slight

increase in fiber diameter, while a decrease at 4 wt% MWCNT suggests that the dominant effect of increased electrical conductivity at higher loadings can overcome viscosity, promoting finer fiber formation. The electrospun fibers' high porosity and surface area contributed to excellent filtration, further improved by MWCNTs acting as capture sites and stabilizing the fiber structure. Thermal analysis revealed MWCNT influences on crystallization and stability, with low concentrations acting as nucleating agents and high concentrations hindering chain mobility. Mechanical property improvements, particularly tensile strength and Young's modulus were also observed with MWCNT addition.

Based on processability for large-scale production, optimal fiber morphology, comparable filtration efficiency across all MWCNT loadings, and improved breathability with increasing MWCNT content, our novel finding indicates that a 2 wt% MWCNT loading in the electrospun PLA/PBS blend presents the most cost-effective balance for high-performance air filtration. This composition offers good fiber formation, desirable morphology, effective filtration, and enhanced breathability while minimizing material costs associated with higher MWCNT concentrations.

Future research should optimize MWCNT dispersion and loading for further performance enhancement and explore long-term stability and potential in other applications such as water purification and biomedical devices.

Declaration of AI and AI-Assisted Technologies in the Writing Process

The authors utilized Gemini to improve the legibility and clarity of the text during the preparation of this work. The authors assume full responsibility for the content of the publication and review and edit the content as necessary after using this tool/service.

ACKNOWLEDGEMENT

REFERENCES

1. Sangkham S, Phairuang W, Sherchan SP, Pansakun N, Munkong N, Sarndhong K, et al. An update on adverse health effects from exposure to PM2.5. Environ Adv [internet]. 2024;18:100603. Available from: https://doi.org/10.1016/j.envadv.2024.100603.

2. Pai SJ. Carter TS, Heald CL, Kroll JH. Updated world health organization air quality guidelines highlight the importance of non-anthropogenic PM2.5, Environ Sci Technol Lett [internet]. 2022;9(6):501-6. Available from: http://doi.org/10.1021/acs.estlett.2c00203.

3. Selvaranjan K, Navaratnam S. Rajeev P, Ravintherakumaran N. Environmental challenges induced by extensive use of face masks during COVID-19: A review and potential solutions. Environ Challenges [internet]. 2021;3:100039. Available from: https://doi.org/10.1016/j.envc.2021.100039.

4. Villarreal-Gómez LJ, Cornejo-Bravo JM, Vera-Graziano R, Grande D. Electrospinning as a powerful technique for biomedical applications: A critically selected survey. J Biomater Sci Polym Ed [internet]. 2015;27(2);157-76. Available from: https://doi.org/10.1080/09205063.2015.1116885.

5. Phan DN, Khan MQ, Nguyen NT, Phan TT, Ullah A, Khatri M, et al. A review on the fabrication of several carbohydrate polymers into nanofibrous structures using electrospinning for removal of metal ions and dyes. Carbohydr Polym [internet]. 2021;252:117175. Available from: https://doi.org/10.1016/j.carbpol.2020.117175.

6. Dai H, Liu X, Zhang C, Ma K, Zhang Y. Electrospinning polyacrylonitrile/graphene oxide/polyimide nanofibrous membranes for high-efficiency PM2.5 filtration. Sep Purif Technol [internet]. 2021;276: 119243. Available from: https://doi.org/10.1016/j.seppur.2021.119243.

7. Liu H, Zhu Y, Zhang C, Zhou Y, Yu DG. Electrospun nanofiber as building blocks for high-performance air filter: A review, Nano Today. 2024;55:102161. Available from: https://doi.org/10.1016/j.nantod.2024.102161.

8. Yu Z, Fan T, Liu Y, Li L, Liu J, Yang B, et al. Efficient air filtration through advanced electrospinning techniques in nanofibrous materials: A review. Purif Technol [internet]. 2024;349;127773. Available from: https://doi.org/10.1016/j.seppur.2024.127773.

9. Karabulut FNH, Höfler G, Ashok Chand N, Beckermann GW. Electrospun nanofibre filtration media to protect against biological or nonbiological airborne particles. Polym [internet]. 2021;13(19):3257. Available from: https://doi.org/10.3390/polym13193257.

10. Wang L, Gao Y, Xiong J, Shao W, Cui C, Sun N, et al. Biodegradable and high-performance multiscale

structured nanofiber membrane as mask filter media via poly(lactic acid) electrospinning. J Colloid Interface Sci [internet]. 2022;606;961-70. Available from: https://doi.org/10.1016/j.jcis.2021.08.079.

11. Wang Z, Zhao C, Pan Z. Porous bead-on-string poly(lactic acid) fibrous membranes for air filtration. J Colloid Interface Sci [internet]. 2015;441121-29. Available from: https://doi.org/10.1016/j.jcis.2014.11.041.

12. Souzandeh H, Wang Y, Netravali AN, Zhong WH. Towards sustainable and multifunctional air-filters: A review on biopolymer-based filtration materials. Polym Rev [internet]. 2019;59(4):651-86. Available from: https://doi.org/10.1080/15583724.2019.1599391.

13. Hamad K, Kaseem M, Ayyoob M, Joo J, Deri F. Polylactic acid blends: The future of green. Prog Polym Sci [internet]. 2018;85:83-127. Available from: https://doi.org/10.1016/j.progpolymsci.2018.07.001.

14. Phiriyawirut M, Sarapat K, Sirima S, Prasertchol A. Porous electrospun nanofiber from biomass-based polyester blends of polylactic acid and polybutylene succinate. OJPChem [internet]. 2019:9(1):1-15. Available from: http://doi.org/10.4236/ojpchem.2019.91001.

15. Stoyanova N, Paneva D, Mincheva R, Toncheva A, Manolova N, Dubois P, et al. Poly(l-lactide) and poly(butylene succinate) immiscible blends: From electrospinning to biologically active materials. Mater Sci Eng C [internet]. 2014;41:119-26. Available from: https://doi.org/10.1016/j.msec.2014.04.043.

16. Prahsarn C, Klinsukhon W, Padee S, Suwannamek N, Roungpaisan N, Srisawat N. Hollow segmented-pie PLA/PBS and PLA/PP bicomponent fibers: An investigation on fiber properties and splittability. J Mater Sci [internet]. 2016;51:10910–16. Available from: https://doi.org/10.1007/s10853-016-0302-0.

17. Ghosal K, Agatemor C, Špitálsky Z, Sabu T, Kny E. Electrospinning tissue engineering and wound dressing scaffolds from polymer-titanium dioxide nanocomposites. Chem Eng J [internet]. 2019;358:1262-78. Available from: https://doi.org/10.1016/j.cej.2018.10.117.

18. Canales D, Moyano D, Alvarez F, Grande-Tovar CD, Valencia-Llano CH, Peponi L, et al. Preparation and characterization of novel poly (lactic acid)/calcium oxide nanocomposites by electrospinning as a potential bone tissue scaffold. Biomater Adv [internet]. 2023;153:213578. Available from: https://doi.org/10.1016/j.bioadv.2023.213578.

19. Selatile MK, Ojijo V, Sadiku R, Ray SS. Development of bacterial-resistant electrospun polylactide membrane for air filtration application: Effects of reduction methods and their loadings. Polym Degrad Stab [internet]. 2020;178:109205. Available from: https://doi.org/10.1016/j.polymdegradstab.2020.109205.

20. Naebe M, Lin T, Staiger MP, Dai L, Wang X. Electrospun single-walled carbon nanotube/polyvinyl alcohol composite nanofibers: Structure-property relationships. Nanotechnol [internet]. 2008;19:305702. Available from: https://doi.org/10.1088/0957-4484/19/30/305702.

21. Kaur N, Kumar V, Dhakate SR. Synthesis and characterization of multiwalled CNT–PAN based composite carbon nanofibers via electrospinning. SpringerPlus [internet]. 2016;5:483. Available from: https://doi.org/10.1186/s40064-016-2051-6.

22. Zadeh ZE, Solouk A, Shafieian M, Nazarpak MH. Electrospun polyurethane/carbon nanotube composites with different amounts of carbon nanotubes and almost the same fiber diameter for biomedical applications. Mater Sci Eng C [internet]. 2021;118:111403. Available from: https://doi.org/10.1016/j.msec.2020.111403.

23. Alruwaill BM, Saeed U, Ahmad I, Al-Turaif H, Aboalkhair H, Alsaiarl AO. Development of multiwalled carbon nanotube-reinforced biodegradable polylactic acid/polybutylene succinate blend membrane. Membr [internet]. 2021;11(10):760. Available from: https://doi.org/10.3390/membranes11100760.

24. Tian X, Huang Y, Lu Y, Li Z, Liu L, Wang L, et al. Fabrication of an amino-modified MWCNTs grafted with chlorosulfonated PMIA nanofibrous membrane via electrospinning for efficient high-temperature dust filtration. Sep Purif Technol [internet]. 2024;336:126193. Available from: https://doi.org/10.1016/j.seppur.2023.126193.

25. Namsaeng J, Punyodom W, Worajittiphon P. Synergistic effect of welding electrospun fibers and MWCNT reinforcement on strength enhancement of PAN-PVC non-woven mats for water filtration. Chem Eng Sci [internet]. 2019;193:230-42. Available from: https://doi.org/10.1016/j.ces.2018.09.019.

26. Madenli EC, Cakmakci O. Preparation and characterization of PAN/CNT nanocomposite fiber supports for membrane filtration. Desalination Water Treat [internet]. 2017;60:137-43. Available from: https://doi.org/10.5004/dwt.2017.0808.

27. Ghorabi S, Rajabi L, Madaeni SS, Zinadini S, Derakhshan AA. Effects of three surfactant types

of anionic, cationic and non-ionic on tensile properties and fracture surface morphology of epoxy/MWCNT nanocomposites. Iran Polym J [internet]. 2012;21:121–30. Available from: https://doi.org/10.1007/s13726-011-0013-y.

28. Elsharif AM, Bukhari OA. Carbon nanofilms blended with polyvinyl pyrrolidone and Triton X-100 for energy harvesting application. Orient J Chem [internet]. 2020;36(3). Available from: http://dx.doi.org/10.13005/ojc/360306.

29. Pathak R, Punetha VD, Bhatt S, Punetha M. Carbon nanotube-based biocompatible polymer nanocomposites as an emerging tool for biomedical applications. Eur Polym J [internet]. 2023;196:112257. Available from: https://doi.org/10.1016/j.eurpolymj.2023.112257.

30. Khan W, Sharma R, Saini P. Carbon nanotube-based polymer composites: Synthesis, properties and applications. Carbon Nanotubes - Current Progress of their Polymer Composites [internet]. 2016; Available from: http://doi.org/10.5772/62497.

31. Lee JKY, Chen N, Peng S, L Li, Tian L, Thakor N, et al. Polymer-based composites by electrospinning: Preparation & functionalization with nanocarbons. Prog Polym Sci [internet]. 2018;86:40-84. Available from: https://doi.org/10.1016/j.progpolymsci.2018.07.002.

32. Mit-uppatham C, Nithitanakul M, Supaphol, P. Ultrafine electrospun polyamide-6 fibers: Effect of solution conditions on morphology and average fiber diameter. Macromol Chem Phys [internet]. 2004;205:2327-38. Available from: https://doi.org/10.1002/macp.200400225.

33. Xin BJ, Chen W. Morphology, structure and properties of electrospun multi-walled carbon nanotube/polysulfonamide composite nanofibers. J Eng Fibers Fabr [internet]. 2015;10(1). Available from: http://doi.org/10.1177/155892501501000105.

34. Chaiwutthinan P, Pimpan V, Chuayjuljit S, Leejarkpai T. Biodegradable plastics prepared from poly(lactic acid), poly(butylene succinate) and microcrystalline cellulose extracted from waste-cotton fabric with a chain extender. J Polym Environ [internet]. 2015;23:114-25. Available from: https://doi.org/10.1007/s10924-014-0689-0.

35. Nie P, Min C, Song HJ, Chen X, Zhang Z, Zhao K. Preparation and tribological properties of polyimide/carboxyl-functionalized multi-walled carbon nanotube nanocomposite films under seawater lubrication. Tribol Lett [internet]. 2015;58:7. Available from: https://doi.org/10.1007/s11249-015-0476-7.

36. Yuen SM, Ma CCM, Chiang CL, Teng CC. Morphology and properties of aminosilane grafted MWCNT/polyimide nanocomposites. J Nanomater [internet]. 2008;786405. Available from: https://doi.org/10.1155/2008/786405.

37. Chow WS, Lim YT. Antistatic and thermal properties of poly(lactic acid)/polypropylene/carbon nanotube nanocomposites. J Eng Sci [internet]. 2020;16(2):57-69. Available from: http://doi.org/10.21315/jes2020.16.2.3.

38. Ceregatti T, Pecharki P, Pachekoski WM, Becker D, Dalmolin C. Electrical and thermal properties of PLA/CNT composite films. Rev Mater [internet]. 2017;22(3). Available from: http://doi.org/10.1590/S1517-707620170003.0197.

39. Ghane N, Mazinani S, Gharehaghaji A. Comparing the performance of electrospun and cast nanocomposite film of polyamide-6 reinforced with multi-wall carbon nanotubes. J Plast Film Sheeting [internet]. 2019;35(1):45-64. Available from: https://doi.org/10.1177/8756087918794229.

40. Vorawongsagul S, Pratumpong P, Pechyen C. Preparation and foaming behavior of poly (lactic acid)/poly (butylene succinate)/cellulose fiber composite for hot cups packaging application. Food Packag Shelf Life [internet]. 2021;27:100608. Available from: https://doi.org/10.1016/j.fpsl.2020.100608.

41. Eun JH, Sung SM, Kim MS, Choi BK, Lee JS. Effect of MWCNT content on the mechanical and piezoelectric properties of PVDF nanofibers. Mater Des [internet]. 2021;206:109785. Available from: https://doi.org/10.1016/j.matdes.2021.109785.

42. Islam MS, Ashaduzzaman M, Masum SM, Yeum JH. Mechanical and electrical properties: Electrospun alginate/carbon nanotube composite nanofiber. Dhaka Univ J Biol Sci [internet]. 2012;60(1):125-28. Available from: https://doi.org/10.3329/dujs.v60i1.10350

43. Xiao Y, Sakib N, Yue Z, Wang Y, Cheng S, You J, et al. Study on the relationship between structure parameters and filtration performance of polypropylene meltblown nonwovens. AUTEX Res J [internet]. 2020;20(4):366-71. Available from: https://doi.org/10.2478/aut-2019-0029.